Damage Measurements in Epoxy Structural Adhesives using Microhardness

Luis F. Trimiño, Duane S. Cronin*

Department of Mechanical and Mechatronics Engineering,
University of Waterloo, 200 University Avenue West, Waterloo, ON N2L 3G1
ltrimino@uwaterloo.ca, dscronin@uwaterloo.ca

ABSTRACT

The design of adhesively joined components requires the ability to predict and model the joint response under expected operating conditions, including crash events for vehicle structures. Specifically, quantifying adhesive material damage accumulation from static and dynamic loading is essential to predict the response of bonded components in such scenarios. In this study, Vickers microhardness measurements were used as a forensic technique to quantify damage in bulk tensile samples for three structural epoxy adhesive materials: an untoughened epoxy; a toughened epoxy; and a high toughness epoxy. The samples were tested to failure over a range of strain rates (0.002–100 s^{-1}), and hardness measurements were taken post-test along the gauge length. In general, for toughened epoxies the damage extended over much of the sample gauge length, while the un-toughened epoxy demonstrated damage localization at the failure location. The hardness data support the contention that mechanisms such as crazing and shear banding play a role in microhardness changes in toughened epoxies. Increments in strain rate led to an increase in the damage localization. Microhardness measurements were a valuable tool to quantify damage, with the limitation that the magnitude of change in hardness could be adhesive-specific, hypothesized to be related to competing damage mechanisms. The benefits of this approach include the ability to spatially quantify damage, to detect strain rate effects and to carry out measurement of damage post-test in support of constitutive modeling and failure analysis.

Keywords: Damage measurement, Structural epoxy adhesives, Microhardness, Strain rate effects, Crazing, Shear banding

1. INTRODUCTION

Engineering design of adhesively joined components and structures requires the modeling of structural adhesives with appropriate constitutive models to describe the mechanical response and failure under aggressive loading, such as crash scenarios in vehicle applications [1]. The study of adhesives and adhesive joints to support modeling presents challenges as the stress state, strain rates and joint geometry can influence the measured properties and active damage mechanisms in the adhesive [2,3]. Accordingly, quantifying the damage distribution and the relationship to deformation rate is necessary for defining constitutive models that can accurately predict adhesive joint response in bonded components. Adhesives can have a wide range of chemical composition, with epoxies and toughened epoxies commonly used for structural applications. Toughened epoxies are modified to improve the adhesive strain to failure and fracture toughness [4,5], using rubber (butadiene) and high stiffness particles as toughening agents. For example, rubber toughening agents typically comprise particle sizes from 0.1 μm to 0.9 μm in diameter occurring as a suspended phase. However, the particle size depends on the amount of material used for the precipitate and also the relative viscosities between the adhesive components [6,7]. Epoxy adhesive materials can exhibit different deformation and failure mechanisms depending on the mode and rate of loading. In unmodified epoxies, brittle failure is observed, attributed to the existence of microvoids or small stress concentrations in the material [8]. In the case of toughened epoxies, many different mechanisms [5,8] can be active, including: cavitation and fracture of rubber toughening particles; debonding and tearing of other embedded constituents that act like particles (EPM, ABS, polyolefins, etc.); crack deflection by hard particles; plastic zones at crack tips; and shear band/craze interactions. Shear banding and crazing are considered the dominant damage mechanisms for toughened epoxies [9].

Ductile polymers, with strains to failure above 25% [10], typically deform by shear banding, identified by birefringent areas oriented at well-defined angles, typically 45°. Shear bands may initiate at stress concentration points or in areas of high compressive stress. High magnitude localized strains develop within the shear bands [11], without the creation of voids [10].

Crazing, also referred to as strain whitening, occurs through the widening of pre-existing micro cracks as well as the initiation and opening of new cracks in the material [12,13]. Typical craze opening sizes are less than 1 μm in high-impact polystyrene [14], and approximately 2 μm for styrene butadiene-modified polypropylene [6]. The phenomenon may occur at a local area, or may extend along the load-bearing area, depending on the chemical composition of the polymer, microstructure and presence of microdefects [5,6,8]. Thus, crazing can be considered as damage (D) in its most simple interpretation, as the creation and coalescence of voids within a volume of material [15].

Damage may be defined or measured as the ratio between the volume of voids (V_v) and the original material volume (V_o). Similarly, damage can also be defined on an area basis

as the ratio of the area of voids (A_v) to the total area (A_o) of undamaged material in a given cross-section (Equation 1), as proposed by Woo [16].

$$D = \frac{V_v}{V_o} \; or \; D = \frac{A_v}{A_o}$$

Equation 1

Direct measurement of voids is a formidable task, especially if in-situ measurements are desired during loading. Damage is then generally measured by indirect methods, such as [15]: changes in modulus of elasticity; variations in electrical resistivity; changes in wave speed; and changes in hardness. All of these methods are related to the density of the material, and therefore intrinsically related to the voids inside the volume of material. Tang *et al*. [17]measured changes in modulus of elasticity and Poisson's ratio to quantify damage for polystyrene (PS) toughened with rubber particles (HIPS).

The use of microhardness to characterize metals and damage in metallic materials is well established [15,18], but the use of micro-indentation in polymers has been relegated mostly to a simple, non-destructive production control test that indicates cure or chemical composition [19]. Nevertheless, there are studies that demonstrate the flexibility and usefulness of indentation techniques to determine the mechanical properties for viscoelastic materials [20,21], to measure changes in polymeric materials, such as polymorphic transitions due to loading [19], or to identify craze initiation [22]. A possible method, then, to measure the effect of damage in materials is through hardness measurements at discrete points. Hardness can be measured using a standardized scratch hardness test or a Shore Durometer as described in the literature [23], or with the aid of other indentation devices, such as Brinell, Knoop, Rockwell or Vickers. Where indentation size is limited, for example on small samples or thin bond lines, Vickers microhardness is often used [19]. When measuring hardness, damage can be defined in terms of the original hardness of the material (H_o), and the hardness of the material post-loading (H) (Equation 2) [15]. The hardness of a material is often described in test-specific units (e.g. HV), but can be represented using consistent units of force divided by length squared [19]. Typically, results are expressed in units of megapascals, although the measurements do not represent pressure or stress. It is also necessary to consider that the use of Equation 2 does not consider deformation rate dependencies, which are of importance in the description of viscoelastic materials [21].

$$D = 1 - \frac{H}{H_0}$$

Equation 2

Reported hardness values for polymers can be highly dependent on composition, curing temperature, heat treatments and test temperature, with typical values ranging from 30 MPa for poly ethyl-ethylene (PEE) [24] up to 1,000 MPa, as reported by Paplham [25]

for a carbon fiber epoxy composite. The epoxy resin used in Paplham's study had a measured microhardness of approximately 300 MPa. Stoeckel *et al*. [26] and Zheng and Ashcroft [27] have reported microhardness values in the range of 180–220 MPa for different epoxy adhesives. The microhardness of a material can also be estimated, using Tabor's relation [18], as three times the yield strength (σ_y) of the material (Equation 3). This relationship was developed for metals, but has been applied to some polymers [19]. Equation 3 also neglects strain rate effects, therefore it may be limited in application due to the viscoelastic nature of polymeric materials, as demonstrated by Lopez [28].

$$\boldsymbol{HV = 3\sigma_y}$$

Equation 3

Stress-induced changes in microhardness measurements have been reported in the literature, and demonstrate that the material hardness decreases with increasing levels of strain [19,29]. However, it is possible to observe a reversal in this trend, depending on the specific polymer. For example, at high levels of deformation (>40%) PEE microhardness increases, following the notable decrease in microhardness trend for lower strains [24]. The same behavior was reported by Fakirov and Boneva [30] for homo-PBT, but the trend reversal started as low as 10% strain. Baltá-Calleja [19] reports that softening followed by hardening with strain is possible due to "polymorphic" transitions. In such transitions the material changes from an alpha form, in which molecular chains are not fully extended, towards a beta form with chains fully extended. Coiled chains have ductility and produce a lower hardness, while extended chains require more load to deform, hence higher microhardness. In general, for the reviewed literature microhardness measurements made under stress and after unloading are lower compared to the undamaged material, making application of Equation 2 feasible to describe damage in polymers based on microhardness measurements.

In this study, Vickers microhardness was used to quantify damage and damage extent along the loaded zone for bulk tensile samples of three different epoxy adhesives subjected to uniaxial tensile loading until fracture at different strain rates. With adhesive materials, joint geometry and the state of stress can influence material properties, therefore using the bulk material presents a limitation. Nevertheless, the bulk material provides a controlled and repeatable test to further understanding of the active damage mechanisms. It also serves as proof of concept for a methodology that can be extended to more complex scenarios. Additionally, the applicability of Tabor's relationship to epoxy adhesives was explored.

2. METHODS

2.1. Materials and testing

Three different epoxy adhesives (EC-2214, DP-460NS and SA-9850; 3M, Minnesota) were investigated. The selected materials made it possible to compare the response of an

untoughened epoxy adhesive (EC-2214) with a toughened epoxy (DP-460NS) and a material specifically designed for impact resistance (SA-9850). Both DP-460NS (two-part epoxy) and SA-9850 (single-part epoxy) were toughened epoxies with a polymeric phase, while EC-2214 was a single-part epoxy. Table 1 provides a general overview of the chemical composition of each material based on available data from the manufacturer [31]. To quantify the material microstructural inhomogeneity, length scale observations were made for all three materials at intermediate magnification (100–200x) using an opto-digital microscope (ODM) (Keyence VHX-5000) to measure the average size and shape of the visible phases.

Epoxy sheets were manufactured by casting the adhesive material between two glass plates followed by oven curing. Curing temperature and time were set to the manufacturer specifications to develop optimal strength for each material: one hour curing cycle at 120°C for EC-2214; two hours at 70°C for DP-460NS; and one hour at 170°C for SA-9850. Tensile samples were machined from the sheets and loaded in uniaxial tension to failure at different strain rates (0.002, 0.01, 0.1 and 100 s^{-1}). In recent research [1] these materials were identified to exhibit increasing strength and reduced strain to failure with increasing strain rate (Table 2). During uniaxial loading, both DP-460NS and SA-9850 demonstrated strain whitening, but EC-2214 did not (Figure 1).

The DP-460NS material was further investigated for damage features that relate to the strain whitening, such as micro-cracks and shear bands. The toughening agent (butadiene) in DP-460NS is commonly used as a toughening agent [4,6–10], and the particle sizes were comparable to those present in SA-9850. Therefore, this material represented typical feature size relative to the indentation size and, from a Linear Elastic Fracture Mechanics perspective (fracture toughness, Table 2), DP-460NS will generally produce damage features that are larger in size than the non-toughened epoxy (EC-2214) and that are similar in length to SA-9850.

2.2. Microhardness measurements

For this study, the use of a digital Shore durometer was considered (Instron S1 model handheld durometer). However, it was found that the indentation size (1.5 mm in diameter) prevented the possibility of performing a significant number of measurements across the width (3 mm) of the coupon samples for statistical analysis. Nano-indentation could provide better measurement resolution across the width of the samples, and measurements on the order of the size of the damage features. This technique should be considered in the future. The goal of this study, however, was to undertake material hardness measurements at a scale to determine average changes in hardness and material damage. Therefore, a Micro Vickers Hardness Machine (Leco MHD-200 model) was used to measure the material hardness. The device provided repeatable measures and the small indentations (~200 μm) enabled multiple measurements in a small area, required for statistical analysis. The indentations were measured with the optical filar micrometer. At a later stage in the study, measurement of the indentations was undertaken with the ODM to improve measurement consistency. When using Vickers microhardness [19], the

size of the micro indentation diagonal (d) in millimeters and the load applied in Newtons can be related to the hardness of the material (HV) (Equation 4).

$$HV = \frac{1.854 * Load}{d^2}$$

Equation 4

Micro-indentation testing in metals is typically conducted by mounting the specimens in Bakelite or some other support material [32]. In the case of micro-indentation of polymers, Baltá-Calleja [19] and Smith [33] made some recommendations regarding sample mounting and testing. In general, an epoxy resin can be used for mounting polymers because it will have similar mechanical properties as the material to be tested. When mounted in this way, samples need to be cleaned and polished, and a cold-mount resin is required to avoid thermal effects on the material to be measured. To address these challenges, an aluminum support fixture was manufactured to support the samples during the micro-indentation process. A preliminary study was conducted to determine if the support fixture produced results different from those of a sample mounted using an epoxy resin. It was concluded that the use of the support fixture did not influence the hardness results. This same study also determined the ideal load to use during micro-indentation for each material (see Supplementary materials, section 1).

The samples' microhardness was measured before and after uniaxial loading. Three measurements were made in the grip zone before testing, and these served to verify the previously measured basic reference values for each material. To evaluate the effects of loading in the material, microhardness measurements were made in the sample gauge length following uniaxial tensile testing (3 measurements across the width, at 2 mm increments along the gauge length). The indentations started at 0.5 mm from the fracture plane, and a minimum distance of 350 μm was maintained between indentations in the same plane (Figure 2) in order to minimize interaction between measurements.

3. RESULTS

3.1. Epoxy material microstructure measurements

Table 3 summarizes particle size analysis for all three materials. In the analysis, the first phase was the epoxy matrix, and therefore no particle results are reported. In EC-2214 and SA-9850 the micrographs pointed to a microstructure composed of reflective circular particles corresponding to the aluminum aggregates, typically 10 μm in diameter. Dark areas were identified as the elastomeric phase in both materials, with a mean diameter of approximately 20 μm. In both materials, the particle distribution was typically even along the observed surfaces and the particle spacing (edge to edge) was on the order of 10 μm. Although DP-460NS is described by 3 different phases in the chemical constitution (Table 1), it was only possible to identify 2 phases with the ODM: phenol matrix in the background; and a mix of circular and amorphous butadiene, identified as a

darker component. The butadiene particle distribution was random over the material surface; particle separation, measured from edge to edge, varied between 2 μm and 25 μm. It is worth noting that some of the butadiene particles demonstrated internal inhomogeneity (lighter colored areas). This may indicate that the unidentified third silicone phase could be partially distributed within the second phase.

3.2. Strain whitening development in the adhesives

During uniaxial load testing, DP-460NS and SA-9850 showed strain whitening, but EC-2214 did not.

For DP-460NS, as load was applied to the material at very low strain rates, the material first developed small areas of lighter color compared to the base material; the size of these areas grew and coalesced with increasing strain. Eventually, the whitened regions linked and formed inclined bands of whiter color. For DP-460NS, the development of white areas started well before the end of the elastic range (e~0.015) and transitioned towards well-defined bands after reaching the maximum stress (45 MPa); the strain (e~0.03) was below the strain to failure (e≥ 0.10) at this point. At low strain rates, the strain whitening occurred over the entire gauge length of the sample, with development of numerous shear bands. However, as the strain rate was increased, localization of whitening in the vicinity of the fracture zone was identified. After failure there was strain whitening in the gauge for the quasi-static samples, yet it was only noticeable in the region of failure for the high strain rate samples.

In the case of the SA-9850 adhesive, the behavior was similar, although the transition from crazing to shear bands was delayed well into the plastic region with high strains (e≥ 0.05), and the shear bands were not as well defined as in DP-460NS. The whitening was distributed along the entire gauge length of the material sample and was noticeable at all strain rates tested. In SA-9850 the strain whitening was noticeable in the gauge length even after final failure; this was also identified in the high strain rate samples.

3.3. In-situ damage feature measurement in DP-460NS

The DP-460NS material was observed using the ODM during tensile loading to identify the characteristic lengths of features such as micro-cracks and shear bands. The initial typical surface of DP-460NS consisted of the elastomeric phase and pre-existing cracks. From ODM image measurements it was determined that surface defects, such as cracks, were typically less than 3 μm opening. During loading these features could open up to 4 μm. A crack in the sample area imaged began at 26 μm in length and grew to a length of 51 μm under load. It was noted that cracks often coalesced during the loading stage.

Shear band orientation ranged between 28° and 30° relative to the loading direction, and the shear bands were approximately 50 μm in width. Figure 3 illustrates the material surface during load, as well as measurements made on the shear bands and at crack features.

3.4. Microhardness baseline measurements

Microhardness baseline values for each individual adhesive material were established for reference (Table 4). Also reported are the yield strength and the ultimate strength. Values for Tabor's ratio between yield strength and measured microhardness were calculated using Equation 3. The calculation was also performed using the ultimate strength of the materials (Table 5). Micro-indentation diagonal length varied with the materials (Table 4), and in certain cases evaluation with the optical filar was challenging (Figure 4). The ODM facilitated the identification of micro-indentations using variable depth of field imaging and 3D image processing (Figure 5).

3.5. Post-test microhardness and effect of strain rate

The microhardness profile along the gauge length of the sample, beginning at the fracture zone, was determined for the three different materials (Figures 6–8). The figures include box whisker plots that summarize the data at each measurement location. Each box includes a horizontal bar to depict the mean value, the upper and lower fence, and 75% and 25% quartiles. Each figure also includes a corridor indicating the undamaged material mean microhardness values (solid line, data from Table 4) and three standard deviations from the mean (dashed lines).

At each tested location, measurements were compared with those of the undamaged material average microhardness (Table 4), using a T-test with a significance level of 95%. The tables in section 2 of Supplementary materials summarize the analysis results for each material at each measured location. Statistically different locations from the mean are identified with the star symbol in Figures 6–8.

The microhardness measurements were lower, on average, for the tested samples compared to the base material values (Table 4). The EC-2214 material had microhardness values statistically similar to the base material, except near to the fracture zone, while both DP-460NS and SA-9850 exhibited a more even distribution of the microhardness values along the sample gauge length. DP-460NS exhibited wide variability in hardness at the two extremes of the strain rates tested, and at the highest strain rate the average value of microhardness (135 MPa) was higher than that of the undamaged material mean (120 MPa). Due to the variability of the DP-460NS samples at the highest strain rate (100 s^{-1}), the individual samples were investigated in detail to clearly understand the reason for this change and variability (Supplementary materials, section 3, Figure S3-1 and Table S3-1).

3.6. Damage Calculation

From the microhardness measurements (Figures 6–8), and assuming that the material base microhardness was a constant (Table 4), the damage at each measurement location was calculated (Equation 2). Damage values were calculated considering only softened material, which is a limitation of the analysis. The calculated damage was summarized using whisker boxes (Figures 9–11). Note that only information for locations that were statistically significant (identified by * in Figures 6 and 7) was included for EC-2214 and

SA-9850, whereas all of the measured data was used for the DP-460NS damage calculation.

According to the damage calculations from microhardness, for EC-2214 (Figure 9) the average damage value at quasi-static rates was 43%. There was great variability in the calculated damage and the reported values could be as low as 15% and as high as 66%. Moving away from the fracture zone the calculated damage always decreased. At the next strain rates (0.01 and 0.1 s^{-1}) the trend was repeated, with higher damage detected towards the fracture zone than in the furthest location reported. Two trends in the calculated damage were noticed: with increases in strain rate the amount of damage decreased; and increasing difference between the value at the fracture zone and the other locations was also detected.

In the case of SA-9850 (Figure 10), the calculated damage value varied around an average of 37% and was independent of strain rate up to a strain rate of 0.01 s^{-1}. The damage was more or less distributed evenly along the length gauge of the specimens, although increased variability and trends towards lower values were detected further away from the fracture zone. At higher strain rates, localization began to appear in the vicinity of the fracture zone and the calculated damage was reduced to 25% on average. The samples at 0.1 s^{-1} had a trend not noticed anywhere else. For this data the calculated damage was greater further away from the fracture zone (30% in average), than closer to the fracture zone (20% on average). Further review of the microhardness values (Figure 7) indicated that for this particular sample group, there was a reverse in the microhardness trend close to the fracture zone.

The DP-460NS damage data (Figure 11) reflected a trend towards higher damage in the region of the fracture zone. The calculated damage was 20% on average closest to the fracture zone for all strain rates. The damage was typically greater towards the fracture zone and then tapered off towards a lower value (5–10%) moving away from the fracture zone. At the highest strain rate tested (100 s^{-1}), the damage closest to the fracture zone was also around 20% on average, but there was variability along the gauge length. Fluctuations between 16% and 25% in average value were detected in these zones. Finally, at the furthest location average damage was calculated as 10%.

4. DISCUSSION

4.1. Measurement of microhardness in epoxy materials

The traditional equipment used to measure microhardness can have difficulty identifying indentations in certain materials, specifically polymeric materials with aggregates that appear dark under microscope light (Figure 4, SA-9850 and EC-2214 materials). Although measurements with a filar micrometer and a regular confocal microscope were possible, it required high skill, and in some cases it proved challenging to properly identify the location or the boundaries of the indentation. Identification can be enhanced with the use of a contrasting medium (marker ink), but this approach remains limited

because while it can aid in identifying the presence of an indentation, it cannot clearly delineate the boundaries. In this study, an opto-digital microscope (ODM) was used to verify previous measurements gathered with traditional filar micrometer and regular confocal microscope imaging. Importantly, the ODM capability to measure surface profiles facilitated the identification and measurement of indentation features (Figure 4 far left vs. Figure 5), especially in low contrast conditions.

4.2. Length scales

The damage calculations assumed that each adhesive could be treated as a continuum. Such an assumption must be supported by demonstrating that the material microstructure, inhomogeneity and the length of the damage features were sufficiently smaller than the size of the microhardness indentation.

For the EC-2214 and SA-9850 adhesives, the material microstructure can be considered as an aggregate of particles (Figure 4, center and far right). Such particles were typically circular in shape and 3–37 μm in diameter (Table 3). In DP-460NS, micrographs showed a random distribution of the elastomeric phase in both particle shape and size. Particle analysis in this material identified sizes up to 22 μm in diameter in the observed region. Measurements of damage features identified features in DP-460NS up to 4 μm in width and up to 50 μm in length, while shear bands were typically 50 μm in width and oriented at 30°. The measurements were reasonably close to the reported data in the literature for crazing crack openings, on the order of 1–2 μm [7, 17–20] in different polymeric materials. From a fracture mechanics perspective, given the similarity in mechanical properties (Table 2) and particle sizes (Table 3) across the toughened materials (DP-460NS and SA-9850), the reported crack sizes should be a representative length scale of damage features for both materials. For the regular epoxy (EC-2214), given the lower fracture toughness, the characteristic length of damage features are expected to be smaller than the measured values in DP-460NS. Microhardness indentation sizes ranged between 140 μm and 316 μm (Table 4) in diagonal length. Typical micro-indentations are depicted in Figure 4 inside the red circle. From the ODM results (Figure 5), a value of 6 μm can be considered as a representative magnitude of the indentation depth. The microhardness diagonal length scale is at least 3 times larger than the largest microstructure features, and ~ 300 times larger than the smallest features in the material. Not considering the depth of indentation, the materials could be treated as a continuum for damage characterization and interpretation of the hardness measurements.

4.3. Measured microhardness values

Microhardness measurements made in the undamaged materials were lower than the typical expected range for epoxy resins (~ 300 MPa), but this can be expected as the tested epoxy adhesives incorporate different levels of elastomeric materials in their chemical composition. The EC-2214 epoxy with the lowest amount of toughening agent (< 5% per weight) exhibited the highest microhardness (250 MPa). This value is below that reported by Pahlman [25], but well within the approximate expected range of epoxy materials (165–300 MPa). Both DP-460NS (120 MPa) and SA-9850 (102 MPa) had a

higher content of toughening agent, which was reflected in lower microhardness measurements. Tabor's relation was also evaluated using the undamaged material measured microhardness and compared to the measured yield strength and ultimate strength. For all three materials the calculated ratios were between 3.3 and 4.7 using the yield strength, and between 3 and 4 using the ultimate strength. Given these values, we consider that the Tabor relationship can provide a reasonable approximation of the strength for the epoxy adhesives examined in this study. Conversely, since yield values for polymeric materials are scarce in the literature, the ultimate strength could be used to obtain a reasonable approximation for the microhardness of the material when needed. Baltá-Calleja [19] linked microstructure with the Tabor findings and explained that materials with hardness to strength ratios close to 3 are representative of polymers with high crystallinity. Clearly, the measured ratios in this case cannot be interpreted in terms of crystallinity alone because epoxy resins are generally considered to be amorphous glassy polymers.

4.4. Strain rate effects on the microhardness

The microhardness indentation data were used to investigate the effect of strain rate on the hardness of the structural epoxy adhesive materials.

In general for the EC-2214 material, changes in microhardness were highly localized at the fracture zone and no other statistically significant changes were identified along the gauge length, although variability was present in the results. Microscope observations of the material (Figure 4, middle) show that the micro-indentations can cover regions that include the aluminum additive used in the material formulation, which could play a role in the variability. For the single-part EC-2214 epoxy, the microhardness data (Figure 6) and the T-test analysis demonstrated that for the two lowest strain rates tested (0.002 and 0.01 s^{-1}), the microhardness had lower values at, and adjacent to, the fracture zone. For the 0.1 s^{-1} data, two locations were found to be statistically different from the untested material (Figure 6). However, this result was attributed to sample composition variability and not linked to actual changes in hardness caused by loading. At these two locations the measured microhardness averages (227.95±20.79 MPa and 201.83±35.99 MPa) were within one standard deviation of the virgin material microhardness (251.06±38.04 MPa). A T-test with increased significance level to 99% reports that at the two locations, the microhardness was the same as the base material. Similarly, at the higher strain rate (100 s^{-1}) no statistically significant changes in the measured microhardness were detected.

For the SA-9850 adhesive, the T-test confirmed that the microhardness trend was towards values that were statistically lower than that of the undamaged material (Figure 7). A noticeable change in the material microhardness trend with strain rate was detected: at low strain rates (< 0.01 s^{1}) the microhardness ranged from 60 MPa to 70 MPa, while at higher strain rates microhardness ranged from 70 MPa to 80 MPa. In both cases these fluctuations were statistically different, and lower than the undamaged material microhardness of 102 MPa. They were also statistically different from each other.

Of the three tested materials, the DP-460NS results were most challenging to interpret, a difficulty attributed to the damage mechanisms active during deformation. For the lowest strain rate, the statistical T-values reported both significant and non-significant values, with no observable trend. The changes in significance for the T-values along the test gauge can be explained by the observed changes in the material caused by the loading history. At very low strain rates, the material first experienced crazing, which then transitioned to well-defined shear bands as deformation progressed. During the initial craze formation stage, groups of voids developed that softened the material. As the strain was increased, the development of shear bands caused significant stretch in the polymeric chains, leading to rehardening of the material. The occurrence of these two potentially competing damage mechanisms led to no noticeable changes in the material microhardness (Figure 8). This type of effect in the microhardness, i.e. rehardening with strain, has been reported in the literature for other materials [19,24,30]. The wide fluctuation in microhardness between softer and harder material along the test sample gauge length can be due to pockets of softer crazed material among hardened shear-banded regions, hence the changes in significance for the T-values along the test gauge. It is also important to consider that the many damage mechanisms available for toughened epoxies, as described in the Introduction, can play a significant role in the variability of the measured values. Furthermore, as pointed out by Bucknall [9], differences in particle size can also influence the balance between crazing and shear banding across regions of the material, further complicating the possible reasons for the variability. At the next two tested strain rates (0.01 and 0.1 s^{-1}), the material had less chance to develop a transition between shear banding and crazing, hence the trend in lower microhardness towards the fracture zone. At the highest strain rate, the average microhardness (132.5 MPa) was statistically higher than the material mean microhardness value (Supplementary materials, section 3, Table S3-1, 100 s^{-1} T-test results), although high variability in the data was noted (Figure 8, right). The individual sample measurements (Supplementary materials, section 3, Figure S3-1 and Table S3-1) confirmed the same phenomenon detected in the samples tested at the quasi-static strain rate. For areas where crazing development was evident, the microhardness decreased. At zones where shear bands were present, the microhardness increased.

4.5. Calculation of damage in the epoxy materials

According to the damage calculations from microhardness, the calculated post-test damage fluctuated between 20% and 42% in the materials. Although the average tolerance for damage in EC-2214 (34–42%) seems comparable to the other two adhesives, one has to consider that the calculated damage, according to the statistics, can be as low as 15% in the fracture zone (Figure 9). The concentration of damage in a small area of the test sample and low strains to failure demonstrate the brittle nature of this material. In the case of the toughened epoxies, the damage tolerance was demonstrated by the capacity of the materials to propagate damage along the test sample gauge section. This was propitiated by the capacity of the materials to develop crazing, due to the presence of toughening agents. Calculated damage values along the sample gauge length for both SA-9850 (30–40% damage, Figure 10) and DP-460NS (20% damage, Figure 11)

demonstrated the ability of these materials to tolerate damage across a large area of loaded material. At higher strain rates the capacity to absorb damage was reduced in SA-9850 (20% damage), but remained constant in DP-460NS. Although, at the higher strain rates, DP-460NS demonstrated the initiation of localization, while SA-9850 maintained some of its capacity to tolerate and distribute damage along the test gauge. The differences between low strain rates and high strain rates can be explained by a reduction in the ability of the materials to develop crazing to the same extent as possible during quasi-static loading.

Intuitively, one would expect damage values to be higher in the toughened materials than in the brittle epoxy, as was the case with the PS and HIPS data [17]. In this regard, the shear banding present in the toughened epoxies had a re-hardening effect in the measured hardness value that biased the damage calculation towards a lower result. It is possible to circumvent this issue by extrapolating the undamaged material microhardness – as proposed by Lemaitre [21] for the case of materials where damage and strain hardening occur simultaneously. Using a reference hardness value (H_o) of 300 MPa, typical of a pure epoxy resin, the damage of the toughened epoxies would be on the order of 60–80%, given the range of measured microhardness after failure in both DP-460NS and SA-9850. This is more in accord with the values presented for HIPS [17]. Although the calculated values for damage were not unreasonable for the plain epoxy adhesive (EC-2214), further consideration needs to be given to damage evolution and measurement in toughened epoxy materials (DP-460NS and SA-9850). Both softening and hardening were coupled, and both effects need to be quantified in order to obtain an improved calculation of material damage.

5. SUMMARY

Three different epoxy adhesive materials (EC-2214, DP-460NS and SA-9850 3M, Minnesota) were tested under tensile load at different strain rates and were evaluated using microhardness measurements as a means to measure material damage. Traditionally, micro-indentations for microhardness measurements were measured with a filar micrometer or with the aid of a confocal microscope. In this study, the use of an opto-digital microscope (ODM) was explored and it proved to provide a significant advantage for identification and measurement of microhardness indentations, particularly for low contrast surfaces where the traditional filar micrometer or optical microscopes may not be adequate to measure the size of the indentation. The microhardness measurements demonstrated that changes along the gauge length were dependent on both strain rate and the chemistry of the adhesive. In a non-toughened epoxy (EC-2214), the damage was highly localized around the fracture zone. In toughened epoxies (DP-460NS and SA-9850), the damage extended over much of the sample gauge length and the microhardness variations were linked to the deformation mechanisms, i.e. crazing and shear banding. In these two materials, the shear banding generally increased the measured hardness, while crazing decreased the measured hardness, offsetting one

another and ultimately affecting the damage results. With increments in strain rate, localization increased.

Even though there was a localization effect on the measured damage that prevented measuring hardness, and therefore damage data at high strain rates, microhardness measurements were a valuable tool to quantify damage for epoxy adhesive materials subjected to tensile loading under a wide range of strain rates. The microhardness data along the test sample gauge length were also used to generate damage profiles (Figures 9–11), which cannot be easily obtained by other traditional means to measure damage, such as detecting changes in the modulus of elasticity using load-unload cycles. The Tabor relationship applied to polymeric materials was also explored, and the results suggest that it can be used with toughened epoxy adhesive materials to provide an estimate of strength from hardness values. The microhardness information can be used as an additional verification point for assessing damage prediction capabilities of constitutive models for use in analysis, design and computational models that include adhesive materials.

Acknowledgements: The authors would like to thank 3M Company, Initiative for Advanced Manufacturing Innovation, and Automotive Partnerships Canada for providing financial support for this research. The authors gratefully acknowledge Yogesh Nandwani and Eric Hetherington for their assistance in adhesive material testing.

REFERENCES

[1] Trimiño LF, Cronin DS. Evaluation of Numerical Methods to Model Structural Adhesive Response and Failure in Tension and Shear Loading. J Dyn Behav Mater 2016;2:122–37. doi:10.1007/s40870-016-0045-7.

[2] Georgiou I, Ivankovic A, Kinloch AJ, Tropsa V. Rate Dependent Fracture Behaviour of Adhesively Bonded Joints. Eur Struct Integr Soc 2003;32:317–28. doi:http://dx.doi.org/10.1016/S1566-1369(03)80105-X.

[3] Adams RD, Harris JA. The influence of local geometry on the strength of adhesive joints. Int J Adhes Adhes 1987;7:69–80. doi:10.1016/0143-7496(87)90092-3.

[4] Todo M, Takahashi K, Beguelin P, Kausch HH. Effect of displacement rate on the Mode I fracture behavior of rubber toughened PMMA. JSME Int Journal, Ser A 1999;42:49–56.

[5] Garg, Amar C; Mai YW. Failure Mechanisms in Toughened Epoxy Resins A Review. Compos Sci Technol 1988;31:179–223.

[6] Jang BZ, Uhlmann DR, Vander Sande JB. Rubber particle size dependence of crazing in Polypropylene. Polym Eng Sci 1985;25:643–51.

[7] Pillai JP, Pionteck J, Haessler R, Sinturel C, Mathew VS, Thomas S. Effect of Cure Conditions on the Generated Morphology and Viscoelastic Properties of a Poly(acrylonitrile-butadiene-styrene) Modified Epoxy-Amine System. Ind Eng Chem Res 2012;51:2586–95. doi:10.1021/ie2011017.

[8] Bandyopadhyay S, Science D. Review of the Microscopic and Macroscopic Aspects of Fracture of Unmodified and Modified Epoxy Resins 1990;125:157–84.

[9] Bucknall CB. Quantitative approaches to particle cavitation, shear yielding, and crazing in rubber-toughened polymers. J Polym Sci Part B Polym Phys 2007;45:1399–409. doi:10.1002/polb.21171.

[10] Brostow W. Mechancical properties. In: Mark JE, editor. Phys. Prop. Polym. Handb. 2nd editio, Springer; 2007, p. 423–45.

[11] Bowden PB. The yield behaviour of glassy polymers. In: Haward RN, Holliday L, Kelly A, editors. Phys. Glas. Polym., New York: Wiley; 1973, p. 279.

[12] Berger LL. On the mechanism of craze fibril breakdown in glassy polymers. Macromolecules 1990;23:2926–34.

[13] Andrews EH. cracking and crazing in polymeric glasses. In: Haward RN, Holliday L, Kelly A, editors. Phys. Glas. Polym., New York: New York, Wiley c1973; 1973, p. 394.

[14] Donald AM, Kramer EJ. Craze Initiation and Growth in High-Impact Polystyrene 1982;27:3729–41. doi:10.1002/app.1982.070271009.

[15] Lemaitre J. A course on damage mechanics. Berlin: Springer-Verlag; 1992.

[16] Woo CW, Li DL. A universal physically consistent definition of material damage. Int J Solids Struct 1993;30:2097–108. doi:10.1016/0020-7683(93)90053-A.

[17] Tang CY, Plumtree A. Damage mechanics applied to polymers. Eng Fract Mech 1994;49:499–508. doi:10.1016/0013-7944(94)90044-2.

[18] Tabor D. Indentation hardness: Fifty years on a personal view. Philos Mag A 1996;74:1207–12. doi:10.1080/01418619608239720.

[19] Baltá-Calleja FJ. Microhardness of polymers. Cambridge, U.K.: Cambridge

University Press; 2000.
[20] Oyen ML. Analytical techniques for indentation of viscoelastic materials. Philos Mag 2017;86:5625–41. doi:10.1080/14786430600740666.
[21] Chen X, Ashcroft IA, Wildman RD, Tuck CJ. An inverse method for determining the spatially resolved properties of viscoelastic – viscoplastic three-dimensional printed materials Subject Areas : R Soc London -- Philos Trans 2015.
[22] van Melick HGH, Bressers OFJT, den Toonder JMJ, Govaert LE, Meijer HEH. A micro-indentation method for probing the craze-initiation stress in glassy polymers. Polymer (Guildf) 2003;44:2481–91. doi:http://dx.doi.org.proxy.lib.uwaterloo.ca/10.1016/S0032-3861(03)00110-1.
[23] Mix AW, Giacomin AJ. Standardized Polymer Durometry. J Test Eval 2011;39:103205. doi:10.1520/JTE103205.
[24] Apostolov AA, Boneva D, Baltá Calleja FJ, Krumova M, Fakirov S. Microhardness under Strain. 2. Microhardness Behavior during Stress-Induced Polymorphic Transition in Block Copolymers of Poly(butylene Terephthalate). J Macromol Sci - Phys 1998;37:543–55.
[25] Paplham WP, Seferis JC, Balta Calleja FJ, Zachmann HG. Microhardness of carbon fiber reinforced epoxy and thermoplastic polyimide composites. Polym Compos 1995;16:424–8.
[26] Stoeckel F, Konnerth J, Gindl-Altmutter W. Mechanical properties of adhesives for bonding wood-A review. Int J Adhes Adhes 2013;45:32–41. doi:10.1016/j.ijadhadh.2013.03.013.
[27] Zheng S, Ashcroft IA. A depth sensing indentation study of the hardness and modulus of adhesives. Int J Adhes Adhes 2005;25:67–76. doi:10.1016/j.ijadhadh.2004.02.004.
[28] Lopez J. Microhardness Testing of Plastics : Literature Review 1993;12:437–58.
[29] Boneva D, Baltá Calleja FJ, Fakirov S, Apostolov AA, Krumova M. Microhardness under strain. III. Microhardness behavior during stress-induced polymorphic transition in blends of poly (butylene terephthalate) and its block copolymers. J Appl Polym Sci 1998;69:2271–6.
[30] Fakirov S, Boneva D, Baltá Calleja FJ, Krumova M, Apostolov AA. Microhardness under strain: Part I Effect of stress-induced polymorphic transition of poly(butylene terephthalate) on microhardness. J Mater Sci Lett 1998;17:453–7.
[31] 3M. 3M technical data sheets n.d. http://solutions.3m.com/wps/portal/3M/en_EU/Industrial-Adhesives-Tapes/-/Resources/DataSheets/.
[32] ASTM. Standard E384-16, 2016, Standard Test Method for Microindentation Hardness of Materials 2016.
[33] Smith JW. Fractography and failure mechanisms of polymers and composites. In: Roulin-Moloney AC, editor., London: Elsevier Applied Science; 1989, p. 28.

Figures

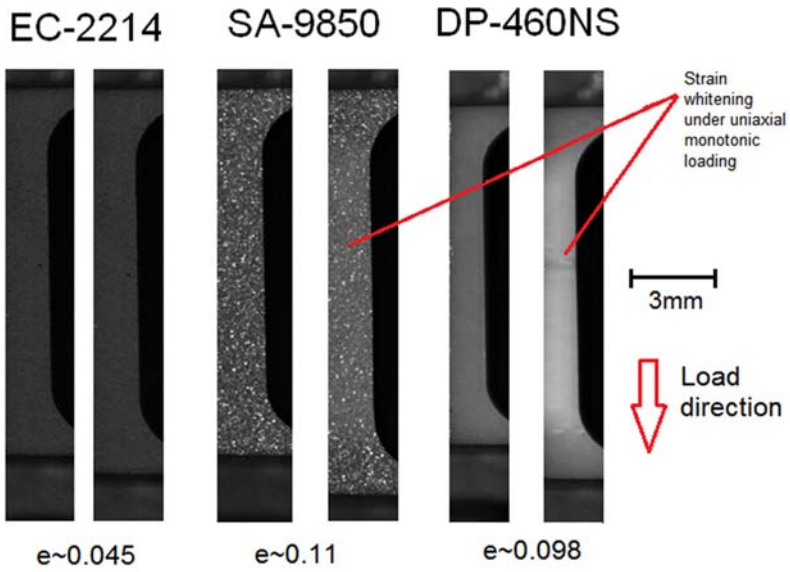

Figure 1: Strain whitening (crazing) for three structural adhesives.

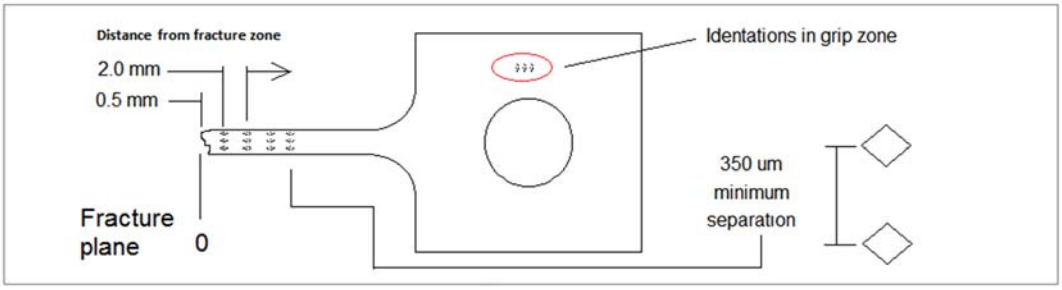

Figure 2: Microhardness measurement locations in samples.

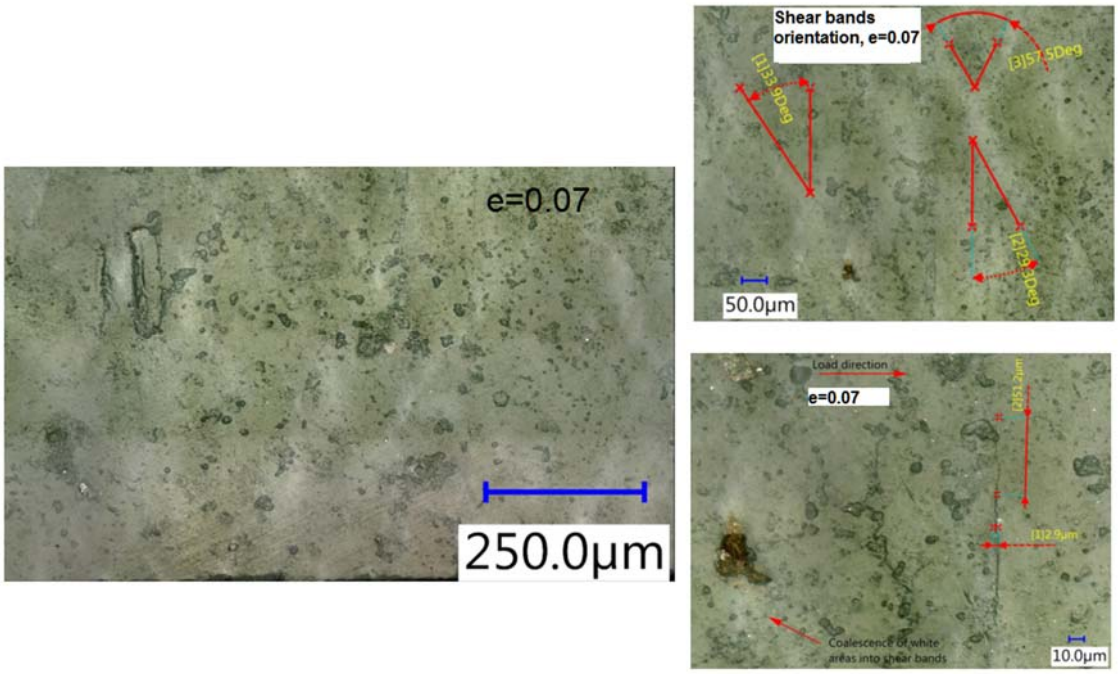

Figure 3: DP-460NS, evolution of surface features and damage under tensile loading.

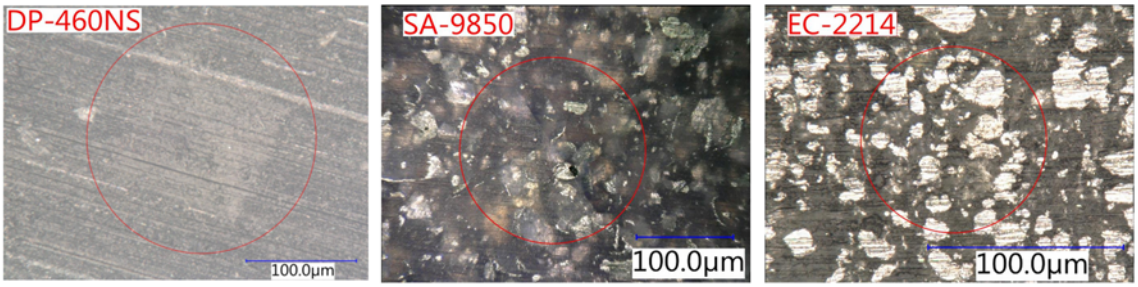

Figure 4: Vickers microhardness indentations in three epoxy materials.

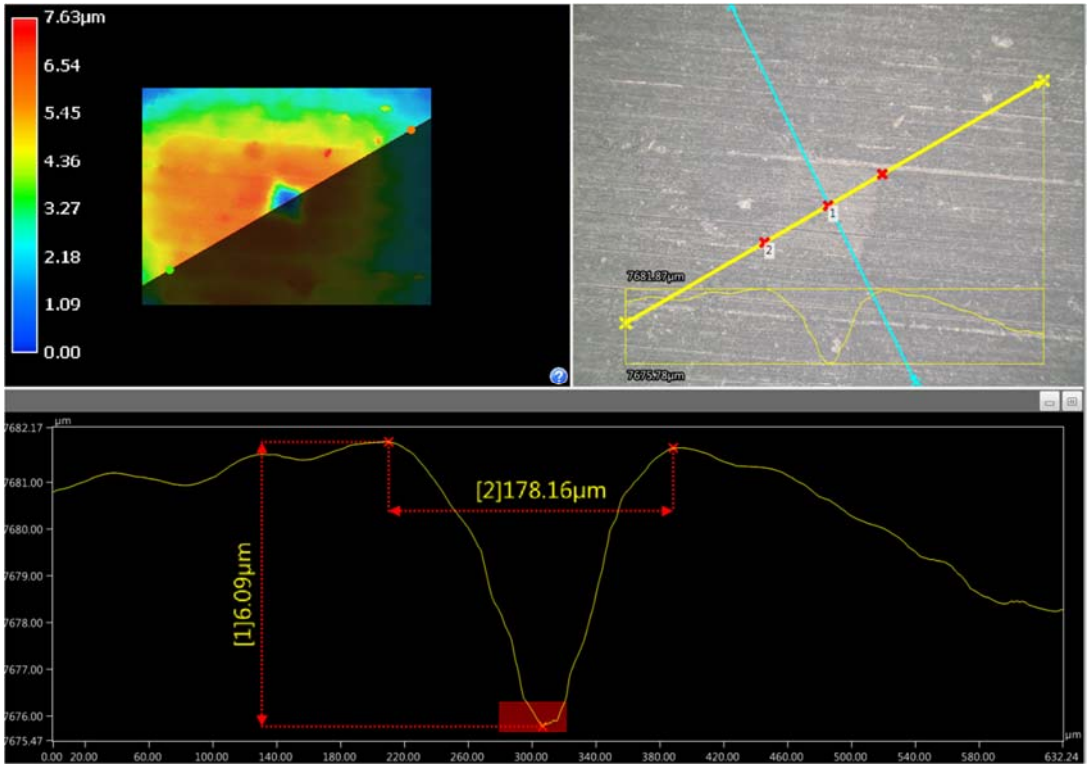

Figure 5: Indentation identification and measurement using an ODM.

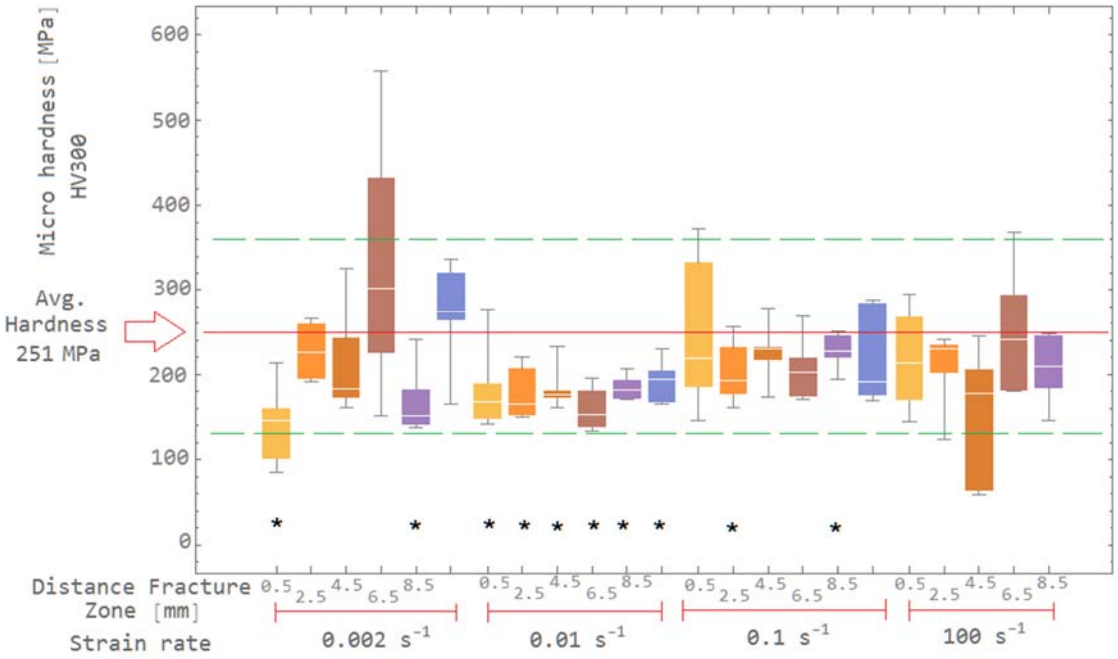

Figure 6: Measured hardness of EC-2214. Undamaged material average microhardness (solid line) with ± three standard deviations (dashed line).

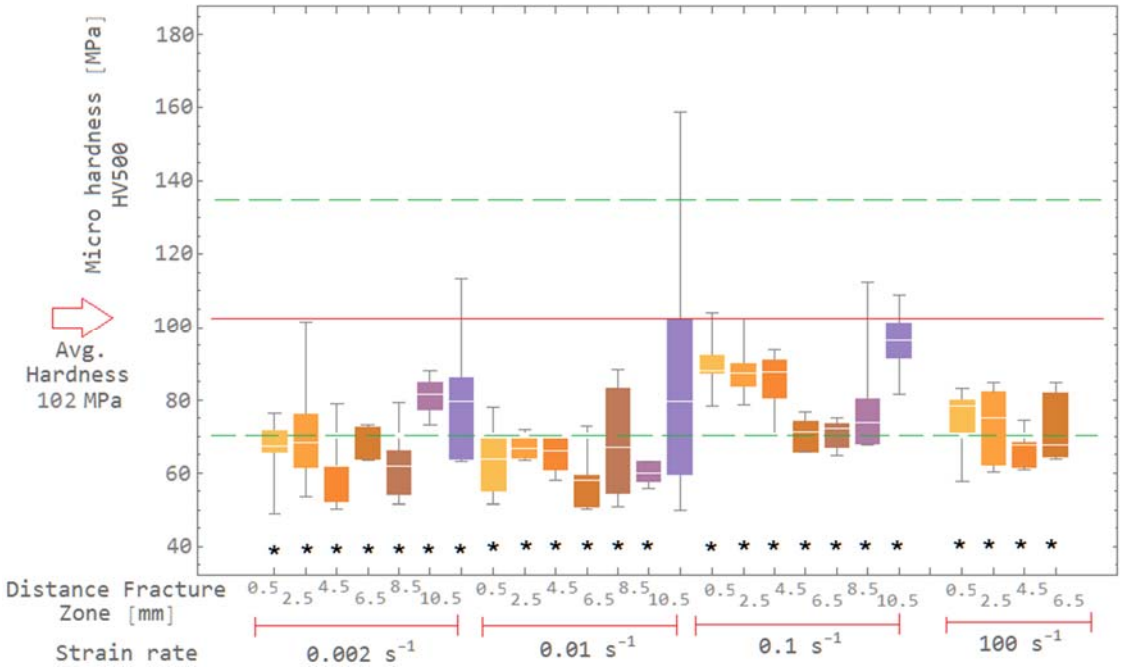

Figure 7: Measured hardness of SA-9850. Undamaged material average microhardness (solid line) with ± three standard deviations (dashed line).

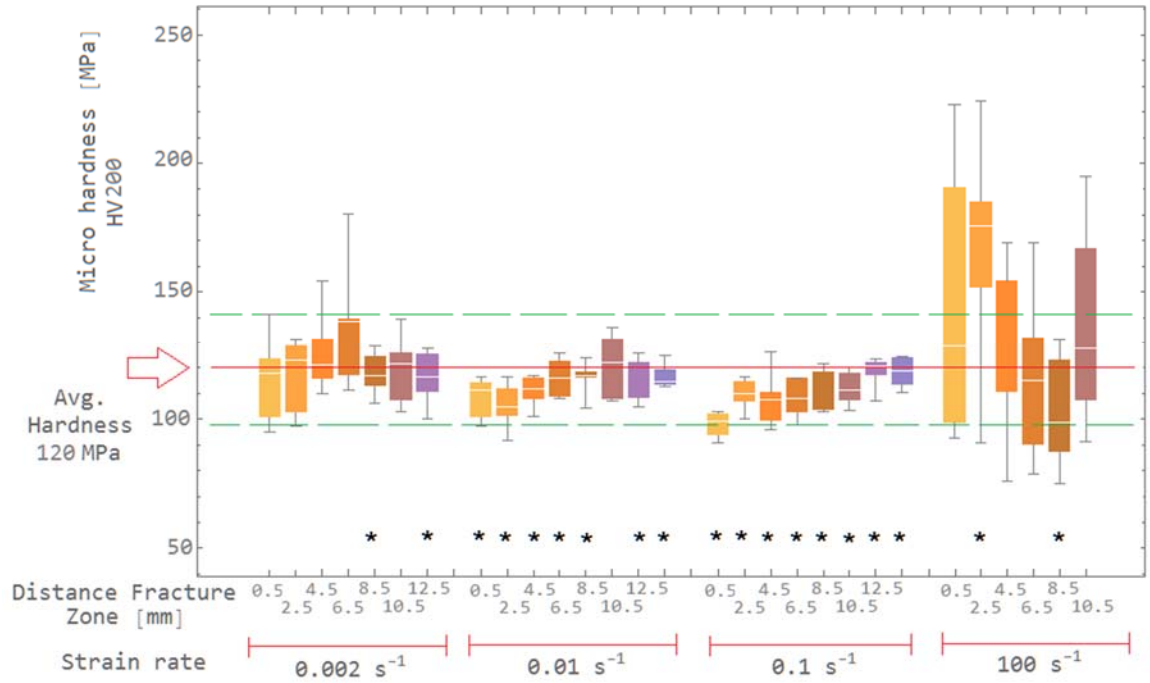

Figure 8: Measured hardness of DP-460NS. Undamaged material average microhardness (solid line) with ± three standard deviations (dashed line).

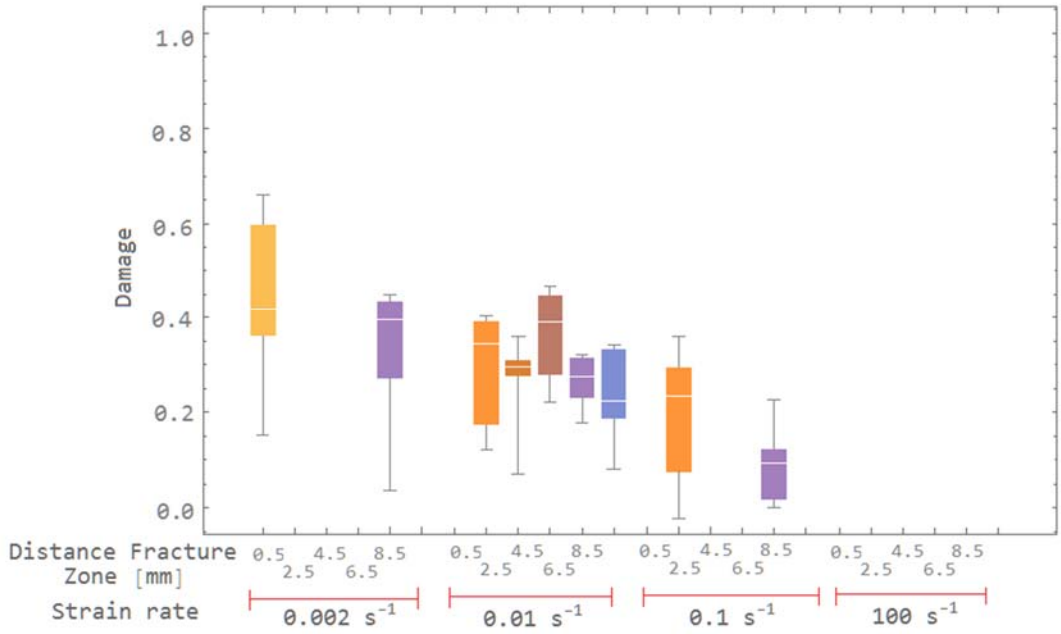

Figure 9: Damage calculated from hardness measurements in EC-2214.

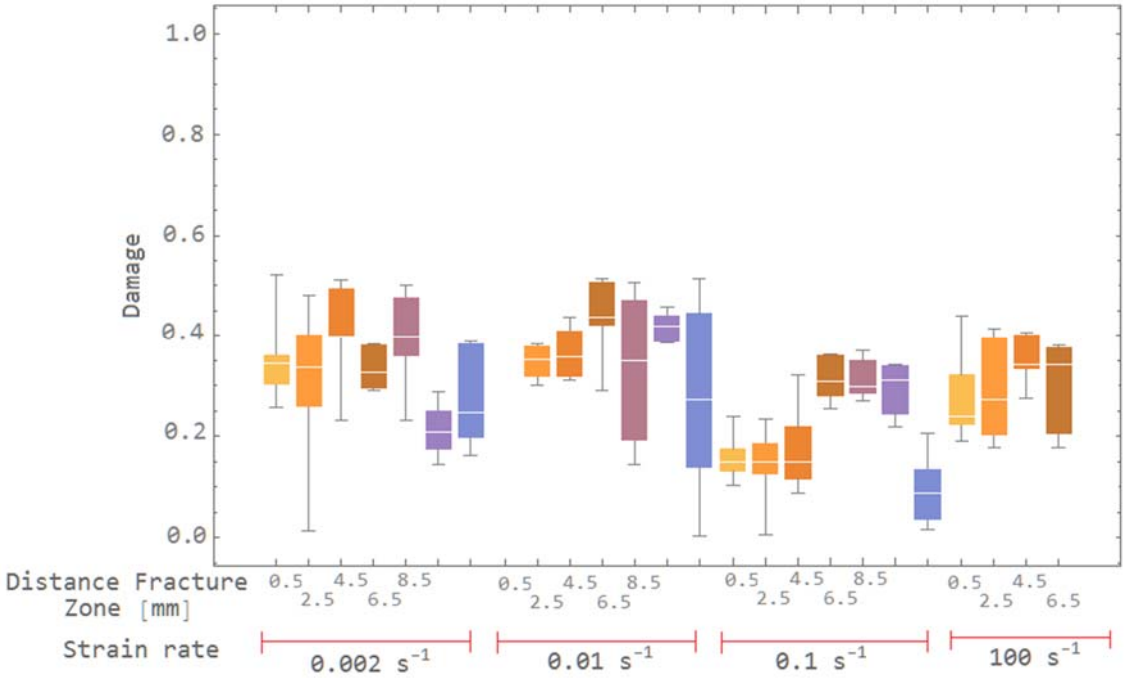

Figure 10: Damage calculated from hardness measurements in SA-9850.

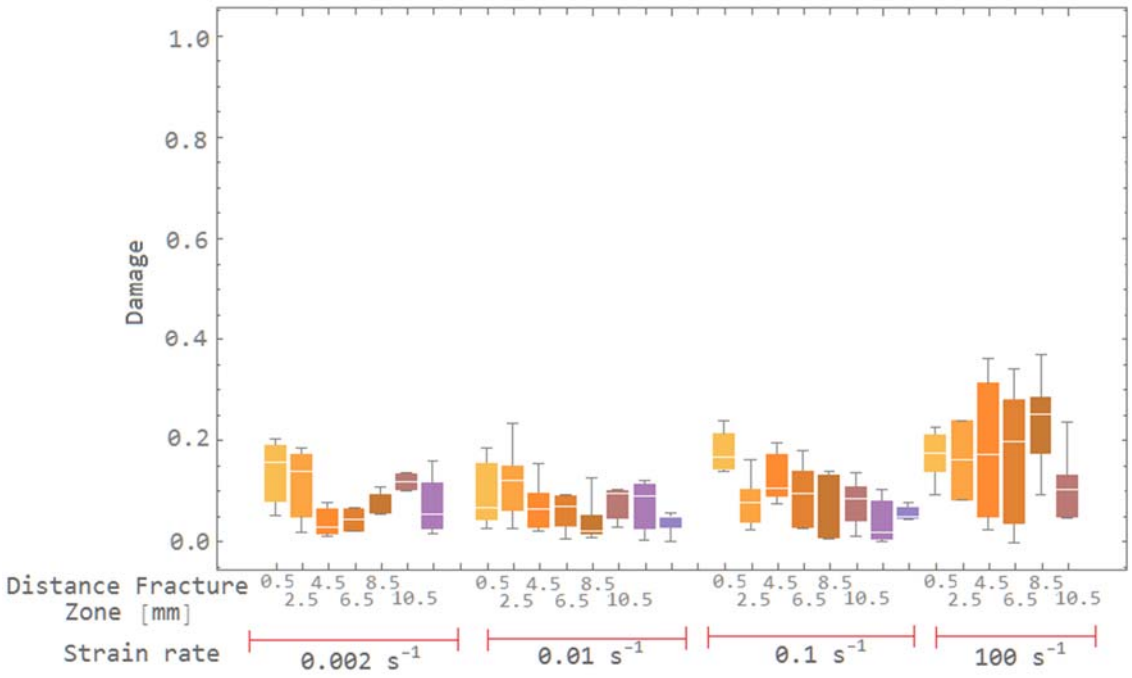

Figure 11: Damage calculated from hardness measurements in DP-460NS.

Tables

Material	Matrix	Phase 2	Phase 3	Phase 4
EC-2214	Epoxy Resin 30–60%	Al pigment 15–40%	Elastomer 1–5%	n/a
DP-460NS	Phenol Resin 60–100%	Butadiene 7–13%	Silicones 1–5%	n/a
SA-9850	Epoxy resin 30–60%	Phenoxy resin 7–13%	Elastomer 10–30%	Al 5–10%

Table 1: Epoxy composition, weight percentages as a ratio of the controlled product.

Material	Density [kg/m^3]	Modulus of Elasticity [GPa]	Poisson's Ratio ν	Tensile Strength Strain Rate Effects [MPa]	Shear Strength Strain Rate Effects [MPa]	GI [MPa/m]	GII [MPa/m]
EC-2214	1540	5.17	0.38	$3.11\ln(\dot{\varepsilon})+83$	$1.91\ln(\dot{\varepsilon})+41$	1.82	5.46

				.53.81		
DP-460NS	1200	2.13	0.41	53.51ln($\dot{\varepsilon}$)+62.9	1.01ln($\dot{\varepsilon}$)+29.3	2.82	10
SA-9850	1200	2.40	0.41	2.71ln($\dot{\varepsilon}$)+46.8	0.41ln($\dot{\varepsilon}$)+26.4	2.97	15

Table 2: Mechanical properties of tested structural adhesives[1]**.**

Material	**Phase 2**	**Phase 3**	**Phase 4**
	Mean Dia. [um]±σ	Mean Dia. [um]±σ	Mean Dia. [um]±σ
EC-2214	17±7	24±9	-
DP-460NS	13±9	-	-
SA-9850	-	10±7	20±17

Table 3: Inclusion size evaluation in the epoxy materials.

Material	Mean Hardness & Std. Dev. [MPa]	Indentation diagonal length & Std. Dev [µm]	Yield Stress [MPa] @ 0.002 s^{-1} [1]	Ultimate Stress [MPa] @ 0.002 s^{-1} [1]
EC-2214	251.06±38.04HV300	150±10.12	53.02	62.32
DP-460NS	120.10±7.20HV200	176±4.96	35.54	39.03
SA-9850	102.90±10.80HV500	301±15.92	24.70	28.24

Table 4: Microhardness of cured structural adhesives prior to testing.

Material	Tabor's HV/Y	Modified Tabor's HV/U
EC-2214	4.73	4.02
DP-460NS	3.37	3.07
SA-9850	4.13	3.64

Table 5: Tabor's relation using yield strength and ultimate strength.

Supplementary materials

Section 1: Preliminary study

A preliminary study was conducted to determine if the fixture support method, to support the samples during micro-indentation, would affect the results compared to an mounting the sample in epoxy mounting resin. Additionally, in all three materials the effect of changes in applied load during the indentation process was studied as micro-indentation results should be independent of applied load.

The DP-460NS sample was mounted in an epoxy resin (NAPA polyester resin, E ~ 3.0 GPa, ultimate strength ~70+ MPa) and measurements were made at different levels of applied weight (200–1000 gr), which were then compared against measurements made in the jig. A T-test statistical analysis demonstrated that the average mean of the support fixture-mounted sample was statistically indistinguishable from the data measured in the epoxy-mounted material (Table S1-1). Additional hardness measurements using the Vickers machine were taken to verify independence from applied load during indentation [18]. In most cases a T-test analysis proved independence of load to be true for DP-460NS and EC-2214 materials (Table S1-1), but there were a few cases where this principle was challenged for SA-9850 (Table S1-1). The data for SA-9850 was plotted in detail (Figure S1-1) and large variability detected only at the two extremes of the loads applied during indentation. The variability of the data in all the adhesives was studied to assess differences (Table S1-2). Much lower variability was present in DP-460NS, and this material microhardness was consistent for all load levels investigated. The variability in the other materials can be related to the inherent error in the measurements since an optical filar micrometer and an optical microscope were used for the measurements at that time, and detectability at the lowest load setting was a challenge. Further investigation with the ODM could be warranted here for SA-9850 and EC-2214, but in general, assuming independence of load to determine microhardness using a Vickers machine is accurate. For each material the load level that provided the least variability in the microhardness results, without compromising appropriate optical detectability, was selected.

Experiment	DP-460NS Epoxy mount vs. Jig	EC-2214 200g vs. 300g	SA-9850 500g vs. 300g	SA-9850 500g vs. 200g	SA-9850 500g vs. 1000g
T_{obs}	2.79	1.38	0.36	4.65	3.59
T_{crit}	3.52	3.30	1.70	1.72	1.71

Table S1-1: T-test statistical analysis with 95% confidence.

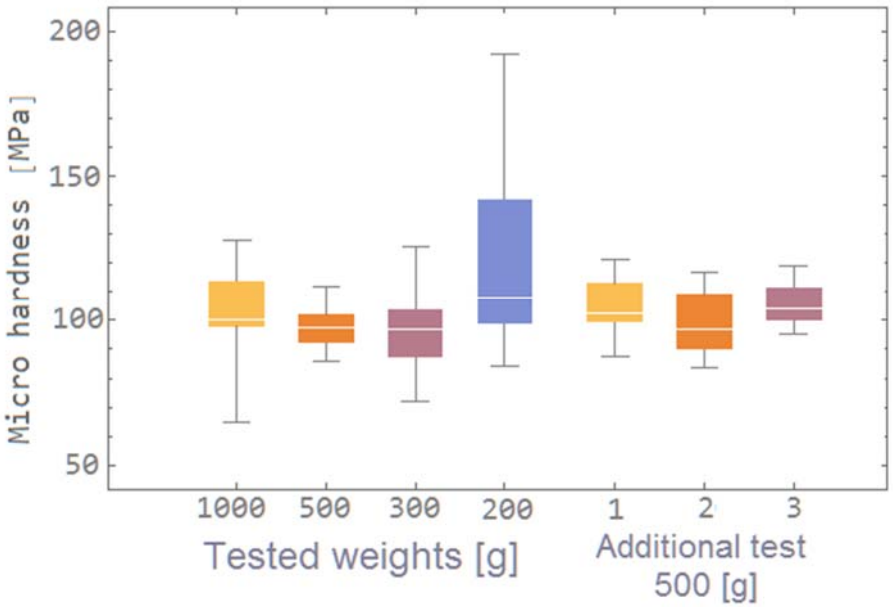

Figure S1-1: Microhardness measurements in SA-9850.

Weight [g]	200	300	500	1000
DP-460NS	10.90	79.52	18.42	24.80
SA-9850	766.92	209.43	72.15	254.34
EC-2214	704.20	1447.11	-	-

Table S1-2: Variance of HV for different applied weights during indentation.

Section 2: Statistical relevance of measured microhardness

The tables below summarize the analysis results for each material at each measured location. Each table contains the observed value (T_{obs}) and the critical value (T_{crit}) for the T-test, with a significance level of 95%. Locations where the mean measured value was deemed statistically different from the material average mean microhardness (Table 4) are marked with the star symbol (*) in Figures 6 to 8. Calculations were made for all three materials for all tested strain rates.

Strain rate [1/s]	**T values**	**Distance from fracture zone[mm]**					
		0.5	2.5	4.5	6.5	8.5	10.5
0.002	T_{obs}	3.03	0.65	0.59	0.11	3.04	0.35
	T_{crit}	1.88	2.06	1.93	2.33	1.85	1.92
0.01	T_{obs}	1.66	4.32	5.03	7.20	7.73	4.44
	T_{crit}	1.89	1.79	1.77	1.76	1.71	1.77
0.1	T_{obs}	0.04	2.13	1.18	1.89	2.14	0.67
	T_{crit}	1.97	1.83	1.81	1.85	1.74	1.91
100	Tobs	0.56	1.17	0.95	0	1.50	-
	Tcrit	1.93	1.87	1.95	1.95	1.85	-

Table S2-1: T-test for EC-2214 measured microhardness values against undamaged material microhardness.

Strain rate [1/s]	T values	Distance from fracture zone[mm]						
		0.5	2.5	4.5	6.5	8.5	10.5	12.5
0.002	T_{obs}	23.09	5.95	22.35	78.14	22.71	20.12	3.43
	T_{crit}	1.89	1.97	1.91	1.75	1.91	2.02	1.97
0.01	T_{obs}	23.40	100	67.72	36.05	7.12	127	0.47
	T_{crit}	1.90	1.71	1.77	1.87	1.97	1.71	2.00
0.1	T_{obs}	8.86	10.76	11.78	67.28	76.65	4.39	3.02
	T_{crit}	1.87	1.87	1.88	1.75	1.73	1.97	1.89
100	Tobs	17.38	144.06	66.56	19.45	-	-	-
	Tcrit	1.89	1.92	1.77	1.89	-	-	-

Table S2-2: T-test for SA-9850 measured microhardness values against undamaged material microhardness.

Strain rate [1/s]	T values	Distance from fracture zone[mm]							
		0.5	2.5	4.5	6.5	8.5	10.5	12.5	14.5
0.002	T_{obs}	1.13	1.02	1.06	1.65	2.97	0.51	2.99	-
	T_{crit}	1.97	1.96	1.97	1.99	1.89	1.95	1.91	-
0.01	T_{obs}	11.95	12.58	14.42	5.52	6.68	0.02	3.50	10.31
	T_{crit}	1.89	1.90	1.87	1.88	1.87	1.94	1.90	1.86
0.1	T_{obs}	49.06	17.36	7.09	12.81	5.86	12.16	3.82	3.96
	T_{crit}	1.86	1.86	1.93	1.89	1.90	1.87	1.87	1.87
100	Tobs	1.12	4.13	1.04	0.76	5.52	1.57	-	-
	Tcrit	1.79	1.79	1.81	1.77	1.77	1.79	-	-

Table S2-3: T-test for DP-460NS measured microhardness values against undamaged material microhardness.

Section 3: DP-460NS analysis at high strain rate (100 s^{-1})

To clearly understand the overall increase in microhardness (132.5 MPa on average vs. 120 MPa) in the undamaged material, and the variability recorded, the individual samples were examined in detail (Figure S3-1). In addition, each sample was subjected to a T-test against the base material measurement (Table S3-1). Sample AF-1 developed mostly crazing, while shear bands weere present only in the area immediately adjacent to the fracture zone, hence the only significant increases in microhardness occurred at this particular point, while all others were softer. The AF-5 sample had crazing followed by mild shear banding along the gauge length, therefore the microhardness measurements were still softer than that of the undamaged material. Lastly, AF-3 developed crazing, but it was followed by a high degree of shear banding and the resultant microhardness was substantially higher. For the three samples tested at the high strain rate, the T-test analysis supported the finding that the changes in microhardness were statistically significant.

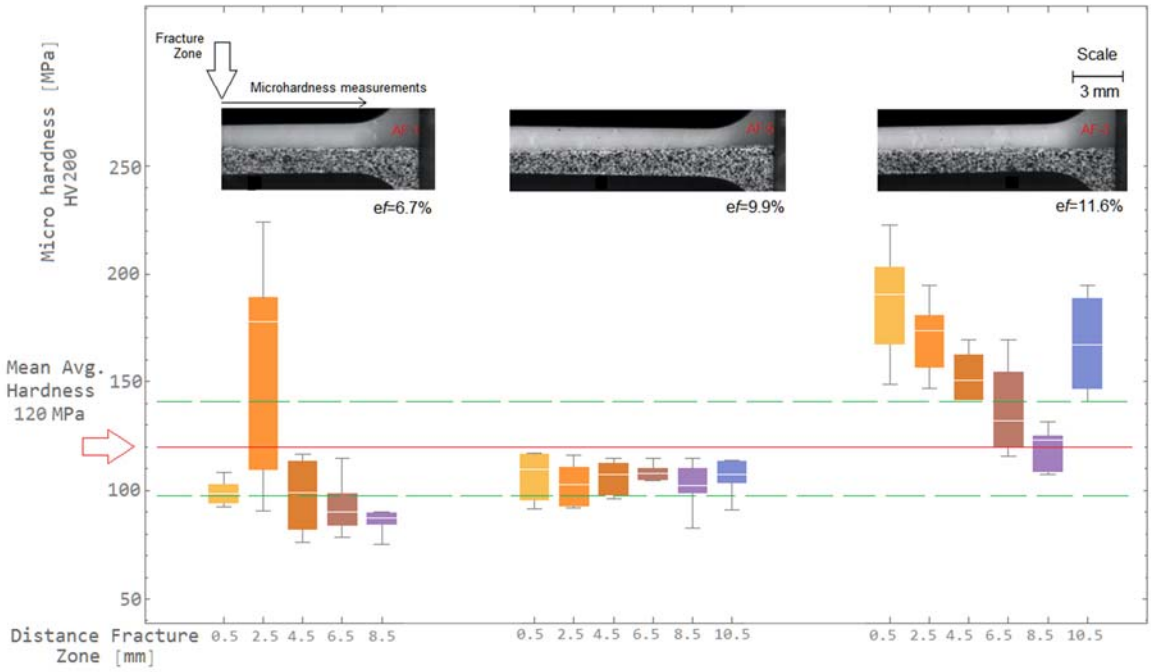

Figure S3-1: DP-460NS individual samples, microhardness measurements at 100 s^{-1} strain rate. Material average (solid line) with +/- three standard deviations (dashed line).

Sample	T values	Distance from fracture zone[mm]					
		0.5	2.5	4.5	6.5	8.5	10.5
AF-1	T_{obs}	28.39	0.96	2.45	9.99	56.97	--
	T_{crit}	1.82	2.01	2.29	1.94	1.79	--
AF-5	T_{obs}	6.69	10.85	13.59	31.59	8.47	11.56
	T_{crit}	1.92	1.89	1.86	1.74	1.92	1.87
AF-3	T_{obs}	5.52	10.17	14.37	2.40	0.19	6.09
	T_{crit}	2.00	1.97	1.92	1.98	1.90	1.98

Table S3-1: T-test DP-460NS individual samples at high strain rate (100 s^{-1}).